Cite this: DOI: 10.1039/c0xx00000x

www.rsc.org/xxxxxx

ARTICLE TYPE

Sub-5 nm Porous Nanocrystals: Interfacial Site-Directed Growth on Graphene for Efficient Biocatalysis

Biao Kong[a,b†], Xiaotian Sun[c†], Cordelia Selomulya[b], Jing Tang[a], Gengfeng Zheng[a], Yingqing Wang[c*] and Dongyuan Zhao[a,b]*

Received (in XXX, XXX) Xth XXXXXXXXX 20XX, Accepted Xth XXXXXXXXX 20XX
DOI: 10.1039/b000000x

The direct production of a macromolecular scale (sub-5 nm) porous nanocrystal with high surface area is a considerable challenge over the past two decades. Here we report on an interfacial site-directed, capping-agent-free growth method to directly produce porous ultrasmall (sub-5 nm), fully crystalline, marcomolecular scale nanocrystals. The porous, sub-5 nm Prussian blue nanocrystals exhibit uniform sizes (~ 4 ± 1 nm), high surface area (~ 855 m^2/g), fast electron transfer (rate constant of ~ 9.73 s^{-1}), and outstanding sustained catalytic activity (more than 450 days). The nanocrystal-based biointerfaces enable unprecedented sub-nanomolar level recognition for hydrogen peroxide (~ 0.5 nM limit of detection). This method also paves the way towards creating ultrasmall porous nanocrystals for efficient biocatalysis.

Introduction

Recent advances in nanotechnology have given rise to a new class of ultrasmall, sub-5 nm nanocrystals[1,2], such as quantum dots[3], carbon nanodots[4,5], graphene nanodots[6], and metal nanoclusters[7]. These sub-5 nm nanocrystals, composed of a few to several hundred atoms, are of significant interest because they provide the missing link between atomic and nanoparticle behavior[8,9]. Their ultrasmall sizes are comparable to the Fermi wavelength of electrons[10], resulting in unusual optical, electrical and chemical properties that differ markedly from larger nanocrystals[11]. Porous materials are of scientific and technological interest with broad applications in catalysis[12], gas separation[13], chemical sensing[14], and optical devices[15,16] due to their large and accessible specific surface areas, tunable and uniform pore sizes, and diverse properties[17,18]. Their abilities to perform desired functions are sensitive to slight variations in the distribution of sizes and volumes of void spaces in the porous frameworks[19,20]. The rational design and fabrication of integrated ultrasmall (sub-5 nm) porous nanocrystals can offer both properties of small size and accessible porosity, leading to a series of tunable functional platforms[21]. Currently, the fabrication of ultrasmall nanocrystals is typically accomplished by solvothermal process[22], cothermolysis method[23], simultaneous precipitation[24], thermal decomposition[25], multiphase mass transfer[26], microwave irradiation[27,28], biomolecule capping[29], and photoreduction[30] strategies. In the most of existing approaches for ultrasmall nanocrystals, the use of suitable reagents capable of stabilizing ultrasmall nanocrystals for enhancing their stability and preventing aggregation is usually necessary. For porous materials, however, the self-assembly of sub-5 nm pore structures is sensitive to the potential changes of assembly conditions[31], especially in the presence of exogenous capping reagents[32], which largely limits the possibility of the synthesis of sub-5 nm pore materials using the existing approaches. Until now, the synthesis of macromolecular scale (sub-5 nm) porous nanocrystals still remains a challenge.

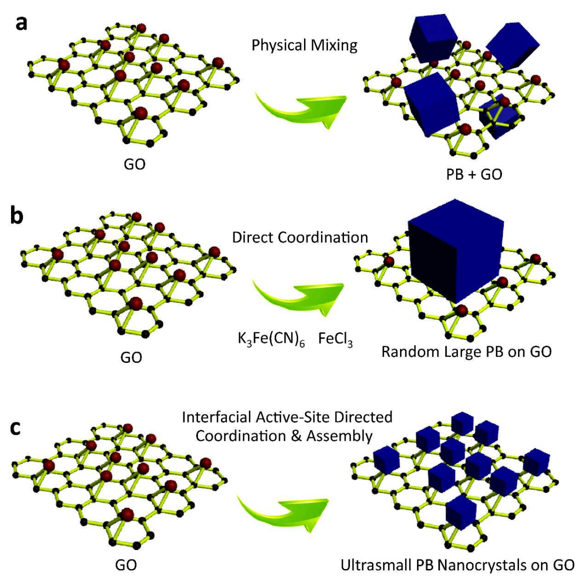

Fig. 1. Comparisons of the classic physical mixing, direct coordination, and interfacial site-directed growth for the sub-5 nm porous Prussian blue nanocrystals. (a) Mixture of Prussian blue and graphene oxide by physical mixing method. **(b)** Random large Prussian blue growth on graphene oxide by direct coordination method. **(c)** Ultrasmall porous Prussian blue assembly arrays on graphene by interfacial site-directed growth method.

Herein, taking the first synthetic coordination compound—Prussian blue (PB, ferric hexacyanoferrate) as an example, we present an atom-level site-directed, capping-agent-free growth of porous sub-5 nm Prussian blue nanocrystals on graphene with a high surface area, ultrasmall size, and narrow size distribution. As a proof-of-concept, the sub-5 nm porous Prussian blue nanocrystals show ultrasmall sizes (< 5 nm), narrow size distribution (4 nm ± 1.5 nm), high surface area (~ 855 m^2/g), ultrafast electron transfer (rate constant of ~ 9.73 s^{-1}), and persistent catalytic activity (more than 450 days), leading to much enhanced catalytic performance (~ 85 fold increase). Specifically, the nanocrystal-graphene heterointerface demonstrates an unprecedented sub-nanomolar level (~ 0.5 nM, limit of detection) for capturing and recognising hydrogen peroxide (H_2O_2) that have never been shown with traditional biointerfaces to date. This approach adds to the synthesis toolbox of nanocrystals and mesoporous materials, creating ultrasmall porous nanostructures from the interfacial site-directed growth that are previously impossible to achieve from traditional approaches. The results should provide an improved understanding of synergistic effect resulting from the integration of small size and accessible porosity, important for developing heterointerfaces for catalysis applications.

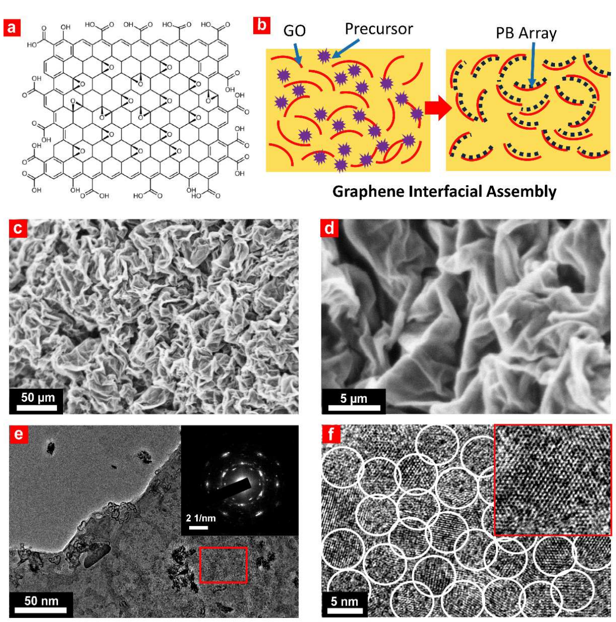

Fig. 2. Characterization of the ultrasmall porous Prussian blue nanocrystals on graphene. (a) A typical amphiphilic graphene oxide structural model with hydrophobic sites (π domains) and hydrophilic sites (-COOH groups). **(b)** Schematic illustration showing the interfacial site-directed growth of ultrasmall porous Prussian blue nanocrystals on graphene oxide. Precursors of Prussian blue nanoclusters was first captured by the active hydrophilic sites and then interacted with the graphene surface for synchronous reduction and growth formation of Prussian blue nanocrystals. **(c-f)** SEM (c, d), TEM (e), and HRTEM (f) images of the obtained ultrasmall porous Prussian blue-graphene composite structure. Inset in Figure (f): The HRTEM image of single ultrasmall porous Prussian blue nanocrystal.

Results

Fabrication of sub-5 nm porous Prussian blue nanocrystals

The interfacial site-directed growth of the sub-5 nm Prussian blue nanocrystals was achieved by controlled hydrolysis, coordination and assembly of molecular precursors on the graphene interface without structure-directing surfactants and capping-agents (**Fig. 2**). Graphene oxide is water dispersity and hydrophilicity, mainly due to a number of hydrophilic oxygenated functional groups (**Fig. 2a**)[33]. Graphene oxide (GO) was synthesized by using a modified Hummers' method and dispersed in water by sonication (4.0 mg mL^{-1})[34]. The precusor of Prussian blue, $K_3[Fe(CN)_6]\cdot 3H_2O$ was slowly added to GO dispersion to form a stable aqueous suspension for pre-interaction of the precursor of Prussian blue and interfacial reactive sites on the GO sheets, following hydrothermal treatment for Prussian blue-anchored graphene nanosheets (**Fig. 2b**). In this way, sub-5 nm porous Prussian blue nanocrystals nucleate and grow on the graphene surface with simultaneous reduction of oxygenated functional groups on the graphene surface. Representative scanning electron microscopy (SEM) images (**Fig. 2c, 2d, Fig. S1**) of Prussian blue-graphene nanosheets show randomly dispersed, crumpled sheets closely associated with each other and forming a highly exfoliated bundle. The transmission electron microscopy (TEM) characterization further validates the successful growth of Prussian blue nanocrystals on the GO sheet. The inset shows the electron diffraction pattern of the as-made Prussian blue-graphene, indicating excellent crystallization of the nanosheets (**Fig. 2e**)[35]. Representative high-resolution transmission electron microscopy (HRTEM) image (**Fig. 2f, Fig. S2**) displays that many uniform nanocrystals of Prussian blue with average sizes of ~ 4.5 nm are homogeneously anchored to the surface of the graphene sheets. HRTEM image reveals a typical single Prussian blue nanocrystal with a well crystalline texture (**inset, Fig. 2f**). The electron dispersive X-ray (EDX) spectra reveal that the presence of Fe component in the Prussian blue-graphene sheets (**Fig. S3a**)[36]. X-ray photoelectron spectroscopy (XPS) showed two peaks at ~ 725 and 711 eV, assignable to Fe 2p1/2 and Fe 2p3/2, respectively (**Fig. S3b**)[36,37]. The Prussian blue nanocrystal-graphene heterostructures are further examined by X-ray diffraction (XRD), which shows clear diffraction peaks of Prussian blue (**Fig. S3c**)[36]. Brunauer−Emmett−Teller (BET) analysis shows that a specific surface area of ~ 855 m^2g^{-1} for Prussian blue-graphene frameworks together with hierarchical porous features.

Fabrication of 3D porous Prussian blue nanocrystal-based hydrogel

The porous Prussian blue-graphene-based 3D hydrogel can be obtained by a hydrothermal assembly at 180 °C for 12 h (**Fig. 3**). The as-prepared hydrogel is directly dehydrated via a freeze-drying process to maintain the 3D monolithic architecture and then used as a biomonitoring interface. The final product from this process is a black monolithic hybrid aerogel composed of graphene networks and Prussian blue nanocrystals (**Fig. 3a**). TEM images reveal an interconnected, 3D porous Prussian blue-graphene frameworks with continuous macropores in the micrometer size range (**Fig. 3b, c**). Apart from the formation of 3D macropores (> 50 µm) on Prussian blue-graphene frameworks by stacking of the Prussian blue-graphene sheets (Figure 2b), a significant stacking pores (~ 10 μm) within the Prussian blue-graphene layers are formed (**Fig. 2c, d**).

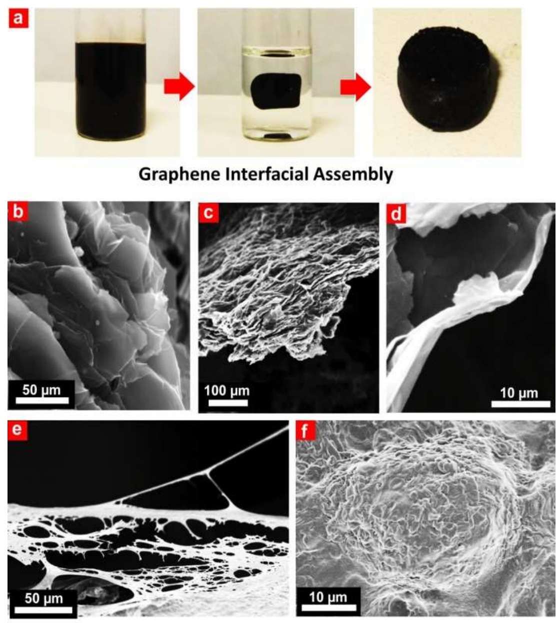

Fig. 3. Ultrasmall Prussian blue nanocrystal hydrogel. (a) Optical photographs of the ultrasmall Prussian blue nanodots-based hydrogels during the formation process. SEM (**b, c**) and enlarged SEM (**d**) images of the obtained ultrasmall Prussian blue nanodots hydrogel. SEM (**e**) and enlarged SEM (**f**) images of the obtained ultrasmall Prussian blue nanodots hydrogel-based cell interface.

Electrochemical performance

Electrochemical interfaces enable fast, low-cost, real time and in situ probing biosignals from living cells and organisms. The electrochemical performance of the porous Prussian blue-graphene heterostructure was investigated by cyclic voltammetry (CV) method. The pristine Ti foil was also measured under a similar condition for comparison. No obvious redox peaks except for the capacitive current are observed for the pristine Ti foil electrode, while the porous Prussian blue-graphene electrode displays a pair of redox peaks at 0.18 and 0.23 V, corresponding to the reversible redox conversion of Prussian blue to Prussian white (**Fig. S4a**). The electrochemical stability of the porous Prussian blue-graphene is also demonstrated by the repeat CV measurements at a scan rate of 50 mVs^{-1}. No observable difference is observed at either the current level or peak positions for CV curves after 200, and 500 cycles, confirming the stability of the immobilized Prussian blue nanocrystals on graphene (**Fig. S4b**). The scan rate dependent voltammetry profile of the porous Prussian blue-graphene electrode in the range 50 − 1000 mV s^{-1} is then presented (**Fig. S4c**). The anodic and cathodic peak potentials of direct electron transfer of Prussian blue are dependent on scan rate (**Fig. S4c**). The anodic and cathodic peak potential shifts slightly in positive and negative directions, respectively. The ΔEp increases with increasing scan rate, however, the value of $E_{1/2}$ is independent on the scan rates. From the dependence of ΔEp on the scan rates, the apparent heterogeneous electron transfer rate constant (ks) is calculated to be 9.73 ± 0.25 s^{-1}, using a surface-controlled electrochemical method[38]. This value of ks is much higher than the most H_2O_2 electrodes reported previously (**Table S1**). It is well-known that the reduced form of Prussian blue presents high catalytic activity for H_2O_2 catalysis. Thus, the capability using Prussian blue-graphene electrode as an amperometric monitoring for H_2O_2 is further investigated.[27] The injection of H_2O_2 (5 mM in a PBS, pH 6.0) leads to a clear increase of current density (corresponding to H_2O_2 reduction), at a lower overpotential (− 50 mV *versus* Ag/AgCl) (**Fig. S4d**). The electrochemical response for hydrogen peroxide reduction depends on the activity of Prussian blue. The open framework of PBs has some interstitial sites and vacancies where counter cations and other small molecules can be intercalated. During this process, Prussian blue nanocrystals act as efficient electron transport mediators between the electrode and H_2O_2 in solution.

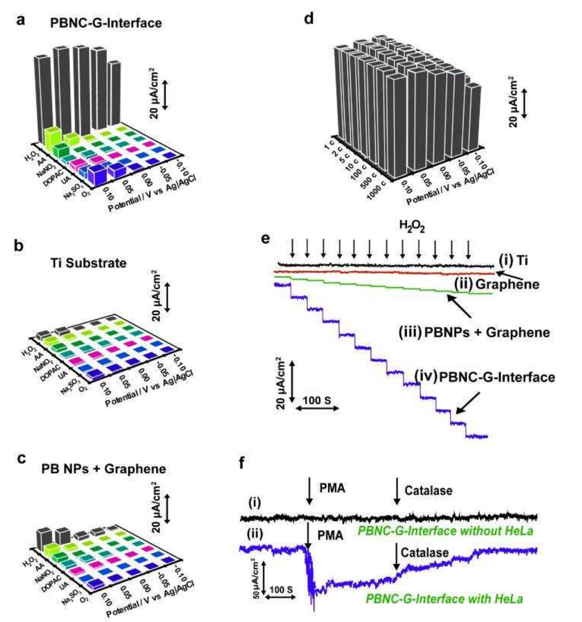

Fig. 4. The performance of porous Prussian blue-graphene (PBG)-cell interface. (a-c) The selectivity and sensitivity profile of the present Prussian blue nanocrystal-graphene-interface (PBNC-G-Interface). (**a**) Current signals from PBG-interface are obtained at different applied potentials: -0.10, -0.05, 0.00, 0.05, 0.10 V *versus* Ag/AgCl. The black Ti substrate (**b**) and traditional mixed PB nanoparticles and graphene (PN NPs + Graphene) interface (**c**) are used as control experiments. (**d**) The stability of the present PBG-interface. (**e**) Typical amperometric responses of the black Ti substrate (**i**), black graphene without PB (**ii**), traditional mixed PB nanoparticles and graphene interface (**iii**), and the present PBG-interface (**iv**) to successive additions of 10 μM H_2O_2 at applied potentials of -0.05 V (versus Ag|AgCl) in PBS (50 mM, pH 6.0). **(f)** Amperometric responses obtained at the blank PBG-interface (**i**) and PBG-interface with HeLa cell (**ii**). The measurements were performed in PBS (50 mM, pH 6.0, with 100 mM of glucose) at the applied potential of -0.05 V (versus Ag/AgCl), after the injection 50 mM of PMA and 300 U mL^{-1} of catalase.

3D porous Prussian blue nanocrystal-based cell interface

The 3D Prussian blue-graphene frameworks as direct growth interfaces of living cells are further demonstrated. The uniform coverage of the ultrasmall porous Prussian blue nanocrystal offers an excellent substrate for the cell attachment and growth, which can subsequently probe different cell functions (**Fig. 3e, f**). The Prussian blue-graphene interface further provides a robust substrate for site-selective cell adhesion and cultivation of living cells, exhibiting high biocompatibility (> 80 %) and excellent biostability towards living cells (up to 120 h) (**Fig. S5**). The biomonitoring performance of the Prussian blue-graphene interface for monitoring of H_2O_2 is extensively investigated. The amperometric responses obtained at the biointerface between the porous Prussian blue nanocrystal-graphene and HeLa cells are measured in 50 mM PBS (pH 6.0) at an applied potential of −50 mV *versus* Ag|AgCl (**Fig. 4**). As the coexisting molecular interferences, such as ascorbic acid, uric acid and so on, may affect the electrochemical monitoring of H_2O_2, the bias potential should be well selected to optimize the cathodic current and sensitivity obtained at the porous Prussian blue nanocrystal-graphene electrodes. Amperometric experiments are carried out to investigate the responses of Prussian blue nanocrystal-graphene toward H_2O_2 at the various potential of −0.10, −0.05, 0.00, 0.05, 0.10 V (versus Ag/AgCl), respectively. Several interference molecules, including O_2, Na_2SO_3, uric acid (UA), 3,4-dihydroxyphenylacetic acid (DOPAC), $NaNO_2$, ascorbic acid (AA) are tested (**Fig. 4a**). In general, low anodic current is obtained for these interference molecules at relatively negative potentials. For example, the ratio of anodic current between H_2O_2 to ascorbic acid (0.1 mM each) is increased from 6.8 to 55, when the applied potential is reduced from 0.10 to −0.05 V (versus Ag/AgCl), leading to an increased selectivity.[31] Hence, −0.05 V (versus Ag/AgCl) is selected as the optimized operational bias potential. In contrast, control experiments of black Ti substrate and traditional mixed PB nanoparticles and graphene interface do not show similar high current signal or signal ratios even at an applied potential of −0.05 V (**Fig. 4b, c**), suggesting that the direct growth and attachment of ultrasmall porous PB nanocrystals on graphene enhance the sensitivity and selectivity. In addition, these data confirm the biomimetic enzymatic amplification nature of the H_2O_2 catalysis at the Prussian blue nanocrystal-graphene interfaces. The long-term stability of the porous Prussian blue nanocrystal-graphene interfaces is displayed by repeating CV cycles at different bias voltages. The Prussian blue nanocrystal-graphene interface maintains 95 % of initial signal responses even after 1000 cycles (**Fig. 4d**). Almost negligible current response is observed at the black Ti substate (**Fig. 4e, line i)**, black graphene without PB (**Fig. 4e, line ii)** at the optimized potential of −50 mV. Amperometric responses of traditional mixed PB nanoparticles and graphene interface (**Fig. 4e, line iii)**, and the present PBG-interface (**Fig. 4e, line iv)** on the successive addition of H_2O_2 are conducted. Stepwise much enhanced current signal correlates well with each addition of H_2O_2 (**Fig. 4e, line iv)**. For the living cell interface, at the injection of 50 mM of phobol 12-myristate-13-acetate (PMA) into the HeLa cell-NW assay, an increase of cathodic current is observed (**Fig. 4f**). No response is observed at the bare Prussian blue nanocrystal-graphene interfaces with the same addition of PMA (**Fig. 4f, line i**). However, an anodic current increase of ~ 65.5 μA is obtained at 15 s (**Fig. 4f, line ii**)[38]. This phenomenon is attributed to the effect of PMA for inducing H_2O_2 production from the cells. Moreover, the injection of catalase solution (300 U mL^{-1} in PBS) leads to the reduction of current level to almost the background, as catalase is known to inhibit the PMA function (**Fig. 4f, line ii**). Accordingly, the increase of cathodic current at the Prussian blue nanocrystal-graphene interface located near the cells is ascribed to the enzymatic reduction of H_2O_2, which is effectively mediated by the ultrasmall porous PB nanocrystal grown on the graphene interface.

Discussion

The synthesis process of the proposed *in-situ* interfacial site directed atom-level assembly on graphene interface without capping-agent is illustrated as follows (**Fig. 5**). The merit of this strategy is that the heterointerfaces could be produced directly from GO in a wet-chemical reaction, where the *in-situ* reduction of GO and growth of ultrasmall sub-5 nm porous Prussian blue nanocrystals occurred simultaneously. The strongly preferred interfacial site directed assembly is due to the fastest reduction and growth at the reactive site of graphene. First, graphene oxide nanosheet is obtained from natural graphite by the well-known Hummers method with minor modification and dispersed in DI water (**Fig. 5a**). Then the *in-situ* assembly of ultrasmall nanocrystals occurs at the water/graphene interface by interfacial interactions of Prussian blue nanocrystal precursors and active hydrophilic sites on graphene surface (**Fig. 5b**).

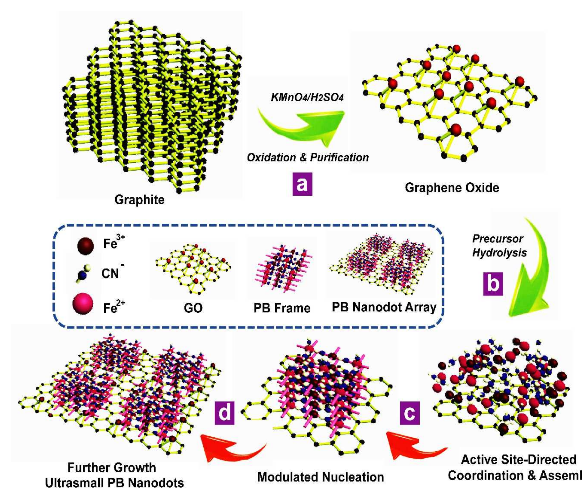

Fig. 5. The proposed growth model of interfacial site-directed assembly for ultrasmall porous Prussian blue nanodots. (a) Graphene oxide is obtained from natural graphite by the well-known Hummers method with minor modification. **(b)** The interfacial interactions of Prussian blue nanocrystal precursors and active hydrophilic sites on graphene surface. **(c, d)** The *in-situ* active site-directed coordination and assembly, modulated nucleation, and further growth of Prussian blue nanocrystals on graphene.

The large graphene nanosheets act as excellent supporters and stabilizers for the Prussian blue nanocrystals. The *in-situ* active site-directed coordination and assembly, modulated nucleation, and further growth of Prussian blue nanocrystals on graphene (**Fig. 5c, d**). As the two reactants have different coordination functionalities, they can only react with the *in-situ* interfacial site directed atom-level assembly on graphene, preventing the formation of aggregates and preserving the porous and single layer structure. This mechanism is also confirmed by two control experiments (**Fig. S7, S8**). No uniform and ultrasmall Prussian blue nanocrystal arrays on graphene are obtained by the same synthesis condition, except that the graphene oxide is removed the most reactive sites (**Fig. S7**) and adding of reduction to mediate the reaction rate (**Fig. S8**).

The porous sub-5 nm nanocrystal-graphene heterointerface possesses several important features. First, the *in-situ* wet-chemical growth route provides a desirable platform for constructing heterointerfaces with improved properties of electron transfer and much enhanced sensitivity. The much enhanced sensitivity of the Prussian blue nanocrystal-graphene is attributed to the unique ultrasmall nanocrystal-graphene heterostructure, in which an intimate contact between the PB nanocrystals and graphene substrate can create synergistic properties of both components. Second, the ultrasmall porous nanocrystals on the surface of graphene can result in the high surface area, persistent catalytic activity and high site-selective cell bioaffinity. The porous PB nanocrystal-graphene interface offers a robust substrate for site-selective cell adhesion and cultivation of living cells, as the porous nanocubes exhibit high selectivity and bioaffinity toward cells, as well as excellent biostability under cell culture adhesion condition (up to 120 h). Meanwhile, the porous heterointerfaces can also serve as long-term stable and sensitive sensing elements for H_2O_2, due to the inherent biomimetic enzymatic activity, high surface area and 3D stereo space based signal molecules touching and recognition.

Compared to the conventional PB-electrochemical interfaces from the physical mixing or direct coordination, the electrocatalytic activity has been enhanced at the Prussian blue nanocrystal-graphene biointerface, due to the rapid charge transport realized by the ultrathin nanostructure of heterointerface and intimate contact between nanocrystals and graphene. Thus, this porous Prussian blue nanocrystal-graphene interface demonstrates a new platform for reliable and durable determination biomolecules from living cells. Importantly, this design of heterostrcututres can be used as other biointerfaces for constructing a serious of electrochemical nanodevices, exhibiting a high sensitivity and long-term stability toward the biomonitoring biomolecules.

Conclusions

In summary, a site-directed, capping-agent-free growth method for porous sub-5 nm nanocrystals on graphene is proposed. As a proof-of-concept, the ultrasmall sub-5 nm porous Prussian blue nanocrystals show narrow size distributions (4 ± 1.5 nm), high surface area (~ 855 m^2/g), fast electron transfer (rate constant of ~ 9.73 s^{-1}), and excellent and persistent catalytic activity (more than 450 days). Specifically, ultrasmall porous Prussian blue nanocrystal-graphene heterointerface exhibits bio-electrochemical, synergistic and selective catalytic functionalities, allowing for unprecedented sub-nanomolar level (~ 0.5 nM, limit of detection) of capturing and recognition for hydrogen peroxide (H_2O_2) that have not yet been demonstrated with the traditional biointerfaces. This approach adds to the synthesis toolbox of nanocrystals and porous materials, creating ultrasmall porous nanostructures from the interfacial site-directed growth. Furthermore, the results should provide improved understanding of synergistic effect resulting from the integration of small size and accessible porosity, important for developing heterointerface for biocatalysis applications.

Notes

[a] *Address: Department of Chemistry, Collaborative Innovation Center of Chemistry for Energy Materials (iChEM), Laboratory of Advanced Materials, Shanghai Key Laboratory of Molecular Catalysis and Innovative Materials, Fudan University, Shanghai 200433, P. R. China*
[b] *Address: Department of Chemical Engineering, Monash University, Clayton, VIC 3800, Australia*
[c] *Address: Department of Cardiothoracic Surgery, Huashan Hospital of Fudan University, Shanghai 200040, P. R. China*

* *E-mail: dyzhao@fudan.edu.cn; wangyiqing@huashan.org.cn*

† These authors contributed equally to this work.

Acknowledgements

This work was supported by the State Key Basic Research Program of the PRC (2012CB224805, 2013CB934104), the NSF of China (81270326, 51273047, 81402917, 21210004, 21322311 and 21473038), Shanghai Sci. & Tech. Committee (14JC1400700), the Australian Research Council (DP120101194, DP140104062), the Deanship of Scientific Research of King Saud University (IHCRG#14-102).

References

1 X. Dai, Z. Zhang, Y. Jin, Y. Niu, H. Cao, X. Liang, L. Chen, J. Wang, X. Peng, *Nature*, 2014, **515**, 96.
2 Y. Li, G. P. Whyburn, Y. Huang, *J. Am. Chem. Soc.,* 2009, **131**, 15998.
3 Y.-P. Gu, R. Cui, Z.-L. Zhang, Z.-X. Xie, D.-W. Pang, *J. Am. Chem. Soc.,* 2012, **134**, 79.
4 A. Zhu, Q. Qu, X. Shao, B. Kong, Y. Tian, *Angew. Chem. Int. Ed.,* 2012, **51**, 7185.
5 S. Zhu, Q. Meng, L. Wang, J. Zhang, Y. Song, H. Jin, K. Zhang, H. Sun, H. Wang, B. Yang, *Angew. Chem. Int. Ed.,* 2013, **52**, 3953-3957.
6 L. Wang, S.-J. Zhu, H.-Y. Wang, S.-N. Qu, Y.-L. Zhang, J.-H. Zhang, Q.-D. Chen, H.-L. Xu, W. Han, B. Yang, H.-B. Sun, *ACS Nano* 2014, **8**, 2541.
7 L. Shang, S. Dong, G. U. Nienhaus, *Nano Today,* 2011, **6**, 401.
8 H. Xu, K. S. Suslick, *Adv. Mater.,* 2010, **22**, 1078.
9 L. Shang, R. Dörlich, V. Trouillet, M. Bruns, G. Ulrich Nienhaus, *Nano Res.,* 2012, **5**, 531.
10 X. Yuan, Z. Luo, Q. Zhang, X. Zhang, Y. Zheng, J. Y. Lee, J. Xie, *ACS Nano,* 2011, **5**, 8800.
11 M. Zhuang, C. Ding, A. Zhu, Y. Tian, *Anal. Chem.,* 2014, **86**, 1829.
12 J. Liang, Y. Jiao, M. Jaroniec, S. Z. Qiao, *Angew. Chem. Int. Ed.,* 2012, **51**, 11496.
13 D.-e. Jiang, V. R. Cooper, S. Dai, *Nano Lett.,* 2009, **9**, 4019.
14 Y. Qin, F. Zhang, Y. Chen, Y. Zhou, J. Li, A. Zhu, Y. Luo, Y. Tian, J. Yang, *J. Phys. Chem. C,* 2012, **116**, 11994.

15 B. Kong, J. Tang, Y. Zhang, C. Selomulya, X. Gong, Y. Liu, W. Zhang, J. Yang, W. Wang, X. Sun, Y. Wang, G. Zheng, D. Zhao, *J. Am. Chem. Soc.,* 2015, **137**, 4260.

16 S. Colodrero, A. Mihi, L. Häggman, M. Ocana, G. Boschloo, A. Hagfeldt, H. Miguez, *Adv. Mater.,* 2009, **21**, 764.

17 C. Galeano, J. C. Meier, V. Peinecke, H. Bongard, I. Katsounaros, A. A. Topalov, A. Lu, K. J. J. Mayrhofer, F. Schüth, *J. Am. Chem. Soc.,*2012, **134**, 20457.

18 Y. Zhao, L. Xu, L. Mai, C. Han, Q. An, X. Xu, X. Liu, Q. Zhang, *PNAS,* 2012, **109**, 19569.

19 N. Zheng, X. Bu, B. Wang, P. Feng, *Science*, 2002, **298**, 2366.

20 X. Fang, Z. Liu, M.-F. Hsieh, M. Chen, P. Liu, C. Chen, N. Zheng, *ACS Nano*, 2012, **6**, 4434.

21 Z. Zhu, S. Wang, J. Du, Q. Jin, T. Zhang, F. Cheng, J. Chen, *Nano Lett.,* 2013, **14**, 153.

22 Y. Chen, J. Ma, Q. Li, T. Wang, *Nanoscale*, 2013, **5**, 3262.

23 G. Chen, T. Y. Ohulchanskyy, R. Kumar, H. Ågren, P. N. Prasad, *ACS Nano*, 2010, **4**, 3163.

24 S. Sarkar, N. S. Karan, N. Pradhan, *Angew. Chem. Int. Ed.*, 2011, **50**, 6065.

25 J. Xie, K. Chen, H.-Y. Lee, C. Xu, A. R. Hsu, S. Peng, X. Chen, S. Sun, *J. Am. Chem. Soc.,* 2008, **130**, 7542.

26 S. A. Khan, S. Duraiswamy, *Lab on a Chip*, 2012, **12**, 1807.

27 J. Tang, Y. Zhang, B. Kong, Y. Wang, P. Da, J. Li, A. A. Elzatahry, D. Zhao, X. Gong, G. Zheng, *Nano Lett.,* 2014, **14**, 2702.

28 W. Lin, K.-S. Moon, C. P. Wong, *Adv. Mater.,* 2009, **21**, 2421.

29 B. Kong, A. Zhu, Y. Luo, Y. Tian, Y. Yu, G. Shi, *Angew. Chem. Int. Ed*, 2011, **50**, 1837.

30 R. Gui, J. Sun, X. Cao, Y. Wang, H. Jin, *RSC Adv.,* 2014, **4**, 29083.

31 Y. Wan, D. Zhao, *Chem. Rev.,* 2007, **107**, 2821.

32 J. Liu, S. Z. Qiao, Q. H. Hu, *Small*, 2011, **7**, 425.

33 B. Kong, A. Zhu, C. Ding, X. Zhao, B. Li, Y. Tian, *Adv. Mater.,* 2012, **24**, 5844.

34 D. A. Dikin, S. Stankovich, E. J. Zimney, R. D. Piner, G. H. Dommett, G. Evmenenko, S. T. Nguyen, R. S. Ruoff, *Nature*, 2007, **448**, 457.

35 B. Kong, J. Tang, Z. Wu, C. Selomulya, H. Wang, J. Wei, Y. Wang, G. Zheng, D. Zhao, *NPG Asia Mater.,* 2014, **6**, e117.

36 B. Kong, J. Tang, C. Selomulya, W. Li, J. Wei, Y. Fang, Y. Wang, G. Zheng,; D. Zhao, *J. Am. Chem. Soc.,* 2014, **136**, 6822.

37 B. Kong, J. Tang, Z. Wu, J. Wei, H. Wu, Y. Wang, G. Zheng, D. Zhao, *Angew. Chem. Int. Ed.,* 2014, **53**, 2888.

38 C. Cai, J. Chen, *Anal. Biochem.,* 2004, **325**, 285.